AL-ZAHRAA UNIVERSITY JOURNAL
Health and Medical Science

Al-Zahraa Journal for Health and Medical Sciences 2025; 3:1-24 Vol. 3, No.1, 2025
www.zjhms.alzahraa.edu.iq

Water pollution treatment using $CoFe_2O_4$ /AC/PANI as a ternary nanocomposite: Kinetic and Thermodynamic study

Mohammed F. Hateef [1,2*], Hasan F. Alesary [2], Stephen Barton[3]

[1] Oil Department, College of Engineering, University of Kerbala, Karbala, Iraq.
[2] Department of Chemistry, College of Science, University of Kerbala, Karbala, Iraq.
[3] School of Life Sciences, Pharmacy and Chemistry, Kingston University London, Kingston-upon-Thames, Surrey, UK
*mohammed.fadhil@s.uokerbala.edu.iq

Received: 10 January (2025), Accepted: 29 February 2025. Published: 31 March. 2025

ABSTRACT

The research assessed the effectiveness of removing the harmful anionic Direct orange 39 dye using $CoFe_2O_4$/AC/ PANI nanocomposite as a novel and economical nanoadsorbent. This nanocomposite synthesized through chemical coupling and polymerization method for $CoFe_2O_4$ with Active carbon (AC) and polyaniline (PANI). The chemical coupling of composite components performed in ammonium persulfate solutions to create monomer that polymerizations in aqueous acids. Infrared spectroscopy proved the $CoFe_2O_4$ nanoparticles synthesized as an inverse spinel via characteristic peaks between 600 and 400 cm^{-1}, which indicating to the locations of tetrahedral Fe-O and octahedral Co-O. X-ray diffraction conformed that the synthesis ternary composite has nanoscale size 36 nm. The BET surface areas and pore size distribution demonstrated are 54.118 m^2 g^{-1} and 8.9064 m^2 g^{-1}, respectively. The hysteresis loops of adsorption isotherms are type IV, with relative pressure range (P/P_0) of 0.3~1.0, which belongs to type H3 with nanopores. Initially, the adsorption experiment was carried out for this superimposed surface towards the direct orange 39 dye and found high removal dye percentage of 95% at 45 min, surface mass at 0.3 g, and pH 6. The composite surface shows the adsorption kinetics of direct orange 39 dye that can be effectively described by the pseudo-first order model. On the other hand, the thermodynamics functions were detected and found the removal reaction of dye using composite was demonstrated a chemical adsorption (greater than 80 kJ/mol) with endothermic reaction.

Keywords: Direct Orange 39 Dye, Textile Dye, $CoFe_2O_4$/AC/PANI NPs, Adsorption Removal, polymerization.

IRAQI Academic Scientific Journals

Introduction

The modern world has already paid an enormous price in terms of both quantitative and qualitative dimensions due to the rapid socioeconomic advancement in industrial growth that has occurred around the world in the last few decades in terms of quality. Thus, one of the biggest hazards to life on Earth nowadays is the constant increase in environmental degradation.[1-3] The direct release of stable, highly water-soluble, and toxic industrial effluents—such as harmful dyes—into the environment poses a direct threat to public health, among other forms of pollution danger to marine life and human health. [4-6]{Formatting Citation} he presence of both ecotoxicity and health issues for the water organisms and even humans is through, and fishes, invertebrates, and algae are particularly vulnerable to dye hypertension. These compounds can severely undermine the delicate balance of the aquatic ecosystem tissues by inhibiting crucial photosynthesis and respiration. This would lead to loss of biodiversity and disruption of ecosystems processes. [7]. The main industrial sector that pollutes water is the textile industry. The textile sector releases almost 20% of the dyes produced worldwide as waste in industrial effluents. It causes wastewater effluents to include massive levels of unfixed dyes [8,9]. To overcome this problem, aniline was polymerized by mixing it with other materials, such as active carbon and cobalt ferret. Due to its high porosity, wide surface areas, excellent electrical conductivity, strong thermal stability, and great mechanical strength, this composite material has shown promising applications in energy storage devices, particularly in supercapacitors and batteries. Researchers are continuing to explore its potential for enhancing performance and efficiency in various electronic systems., Better dye removal capabilities are achieved by the resultant PANI composites, which are PANI combined with metal oxides and/or carbonaceous materials[10]. The primary goal of this work is focused on the synthesis a ternary nanocomposite $CoFe_2O_4$/AC/ PANI In situ method preparation aa new nano-adsorbent with a large surface area, for removing the direct orange 39 dyes. The characterizations such as XRD, FT-IR, SEM-EDX, Zeta Potential, N_2 adsorption- desorption analysis will detect for conform the synthesize a ternary nano-composite. The kinetic and thermodynamics studies for removal of direct orange 39 using $CoFe_2O_4$/AC/ PANI nanocomposite after conducted: the impact of the adsorbent dosage, contact period, starting dye concentration, and pH solution.

MATERIAL AND METHODS

Anillin was supplied by Zhengzhou Alfa Chemical Co., Ltd Fine Chemicals LLP. Ammonium persulfate ($(NH_4)_2\ S_2O_8$), ferric nitrate ($Fe\ (NO_3)_3 \cdot 6H_2O$) and cobalt nitrate ($Co\ (NO_3)_3 \cdot 6H_2O$) were purchased from Sigma Chemical Corp., USA. Sodium hydroxide (NaOH), and 37% hydrochloric acid (HCl) were supplied from Sigma Aldrich. Direct orange the material was supplied as powder form Hila textile factory. Active carbon was Purchased originating from Carbon Activated Corporation.

Experimental Part

Synthesis of the $CoFe_2O_4$/AC/ PANI

Chemical oxidation polymerization was used to create the $CoFe_2O_4$/AC/ PANI nanocomposite, with HCl and ammonium persulfate (APS) acting as dopants and oxidants, respectively. The oxidant solution of Ammonium persulfate (APS) was prepared by dissolving 9.31 grams of APS in 50 milliliters of 1 M HCl solution ,Exact (1 g) of $CoFe_2O_4$ and (1 g) active carbon (Ac) as ratio (1:1) were added to aniline in ice bath at 0 ^oC, which made beforehand (5 g of aniline, with a density of 1.33 (g/cm^3) in 82 mL of 1 M HCl solution) and mixed using ultra-sonication for 10 min. the final mixture was mixed together in ice bath for 1h at 0 ^oC. In order to fully combined PANI with $CoFe_2O_4$ and AC, oxidant solution of (APS) must gradually add (at ten drops per minute) as a molar ratio of 3:1 using separating funnel to final solution in ice bath at 1-2 ^oC for 1h. This mention conditions were essentially to polymerize the monomers of aniline at 1 to 2 ^oC[11], and change the solution color from dark brown to black suspension. The polymerization reaction was then carried out for an entire night, and the color of the solution was modified from black to dark black- green (oily color) confirming the PANI nanocomposite was produced. The suspension of $CoFe_2O_4$/AC/ PANI nanocomposite was filtered by Buchner funnel, then washed with fresh distilled water. The product was dried under vacuum. The steps of ternary composite synthesis were performed as seen in figure 1.

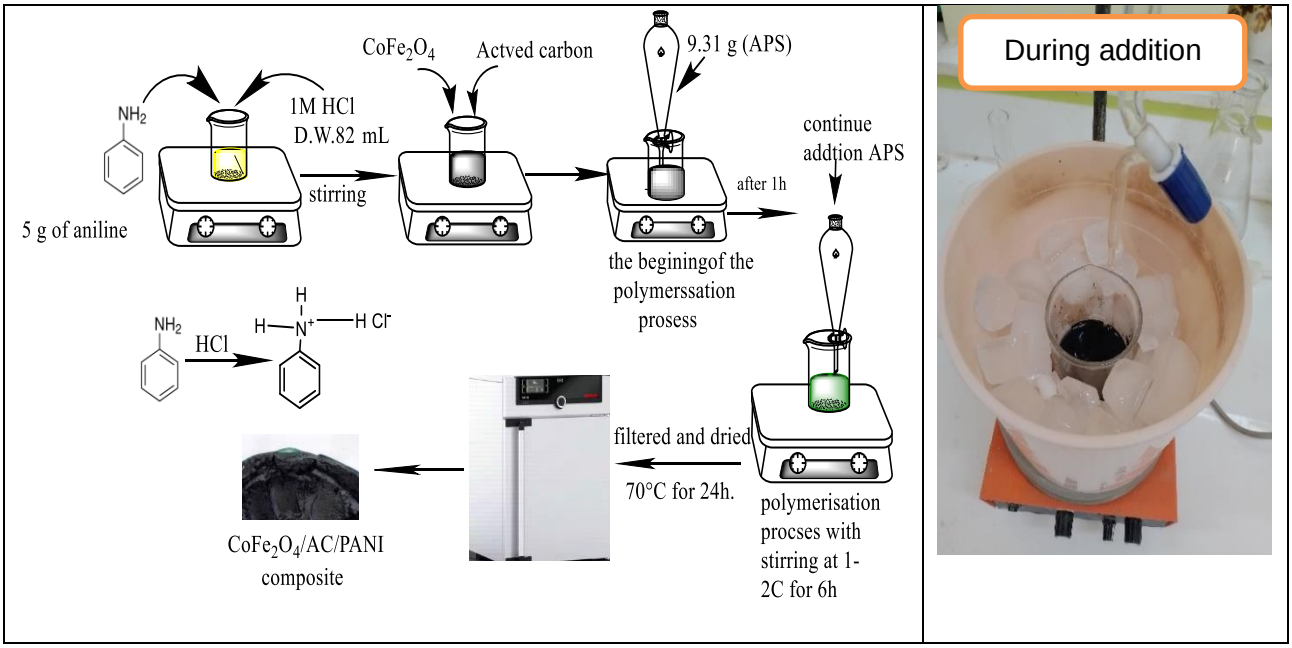

Figure 1. A schematic diagram of the stages involved in producing $CoFe_2O_4$/AC/PANI NPs

RESULTS AND DISCUSSION

CHARACTRIZATIONS

Several investigations, including FTIR, XRD, FE-SEM, EDX-elemental analysis, and BET, were carried out to enable a suitable examination of the samples synthesized in this study. These analyses provided comprehensive insights into the structural, morphological, and compositional characteristics of the synthesized materials. By correlating the results from each technique, a better understanding of the properties and potential applications of the samples was achieved.

FT-IR Analysis

Based on FTIR analysis in figure 2, the red spectrum for $CoFe_2O_4$ detects the stretching vibrations of tetrahedral and octahedral metal oxygen bonding are represented by two stretching frequencies that are detected between 400 and 600 cm^{-1}. The strong stretching vibration peak at a higher frequency of 582.52 cm^{-1} illustrates the tetrahedral sites of (Fe–O), whereas the stretching vibrations of the metal complex (Co–O–Fe) in octahedral sites appears at a lower peak frequency of 470.36 cm^{-1} [12]. These two peaks' existence validates $CoFe_2O_4$ inverse spinel phase[13]. The absorption band at 3124 cm^{-1} was identified as the O-H stretching mode[14] The FT-IR spectrum of

the PANI are displayed in black spectrum. The region of 1528 to 794 cm^{-1} is where the distinctive peaks of PANI are found. The typical C=C stretching of the quinoid and benzenoid rings is responsible for the absorbance peaks at 1572 and 1492 cm^{-1}, whilst the C-N stretching of the secondary aromatic amine is responsible for the band seen at 1295 cm^{-1}. The in-plane bending modes of aromatic C-H are often detected in the range of 1108-1203 cm^{-1}, with a peak at 1149 cm^{-1} and an out-of-plane deformation at 794 cm^{-1}. These vibrational modes provide critical information about the structural characteristics and electronic properties of PANI[15]. Understanding these peaks allows researchers to manipulate the material for various applications, including sensors and conductive polymers. Furthermore, the analysis of these vibrational modes can lead to insights into the polymer's conductivity and stability under different environmental conditions. By correlating the spectroscopic data with the material's performance, scientists can optimize PANI for enhanced functionality in electronic devices [11]. It is worthily mentioned that their intensity and location of the characteristic peaks of PANI change, indicating some chemical interaction between $CoFe_2O_4$ and PANI. In blue spectrum, the presence of 1513.08 cm^{-1} peak in $CoFe_2O_4$/AC/ PANI corresponds to form new bonds due to the combination of three components because this peak does not appear in PAN (black spectrum) or $CoFe_2O_4$ (red spectrum), this peak may be due to the C=N vibrations affected by the interference of AC with PANI. The peak at 786.98 cm^{-1} in spectrum of the ternary compound is associated with the interactions between PAN, $CoFe_2O_4$ and activated carbon. Indeed, the sharp peaks at 470.65 cm^{-1} and 1513.08 $cm^{-1}$are related with the vibrations of Co–O–Fe in octahedral sites[12], and the vibration of C=N, which illustrates the fusion $CoFe_2O_4$ with PAN and AC that enhances the effect of the polymeric structure on the ferrite structure[11,15].

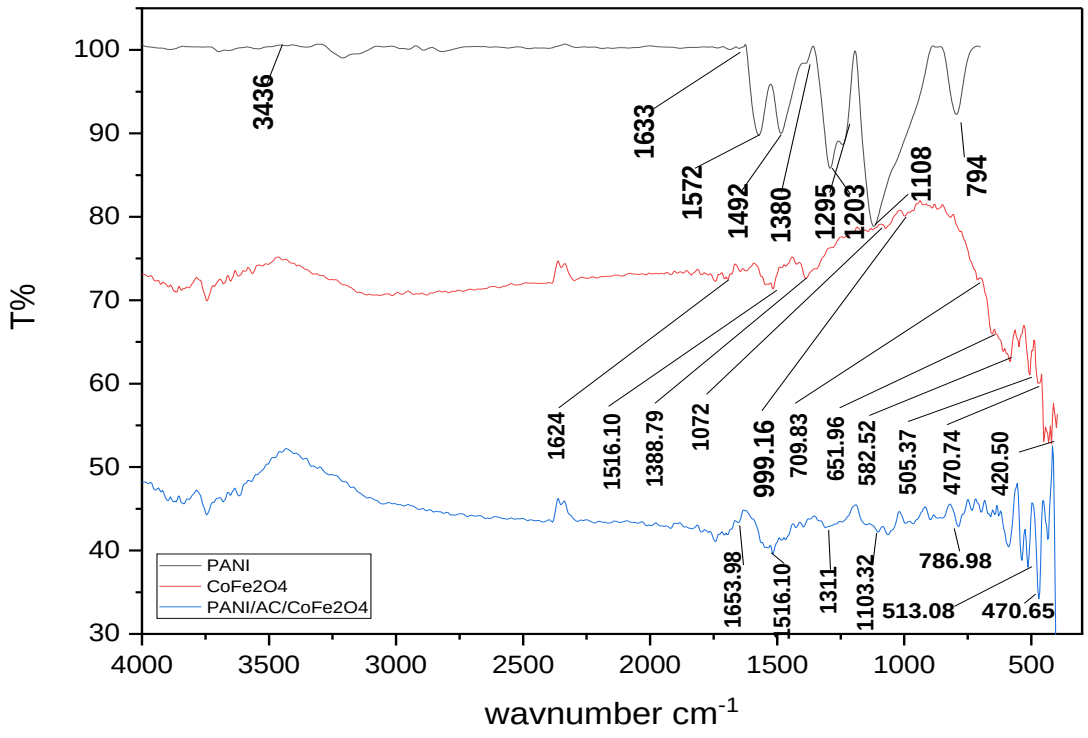

Figure 2. The FT-IR spectra of $CoFe_2O_4$, PANI and composite synthesis.

X-ray diffraction (XRD) analysis

Figure 3 illustrates how Using X-ray diffraction (XRD), The structure of crystals. As can be observed, the active carbon (red line) exhibits broad and weak peaks at 26.1 and 38.5, respectively. These are ascribed to the (0 0 2) and (1 0 0) reflections, and they are consistent with the results of earlier research [16].The XRD analysis of (black line) conformed that the face centered cubic spinel lattice of CoFe2O4 is synthesis according to the diffraction peaks around 2θ =18, 30.45, 35.88, 43.56, 54.17, are attributed to the(111) (220),(311), (222) and (400),respectively (JCPDS -22-1086)[12,17]. The wide peaks in the XRD of PANI (green line) were found at 2θ = 9.10°, 15.23°, 20.87°, and(sharp peak) 75.70° with crystal planes (001), (011), (020) and (200), respectively [11]. The presence of amorphous structure in the PANI matrix was validated by these peaks. The $CoFe_2O_4$/AC/PANI NPs sample contained all of the XRD peaks linked to AC, $CoFe_2O_4$ and PANI when comparing the functional groups of the AC, $CoFe_2O_4$, and PANI samples with the sample of the $CoFe_2O_4$/AC/PANI NPs composite. The structure of the $CoFe_2O_4$/AC/PANI NPs was thus preserved without changes in the crystal planes, with the exception of minor shifts in positions and

variations in the intensities of the associated XRD peaks in comparison to those found in the individual active carbon, $CoFe_2O_4$, and PANI samples. These thus showed that PANI had successfully interacted with AC and $CoFe_2O_4$ In conclusion, our findings support the FTIR data by confirming that PANI was successfully applied to active carbon and $CoFe_2O_4$. The ternary complex's crystalline size was determined by equation [18-21].

$$(L) = \frac{\kappa\lambda}{\beta cos\theta} \qquad (1)$$

where λ is the wavelength of the X-ray radiation source, which is 0.15405 nm, and β is the full width at half-maximum value of the XRD diffraction lines. The Scherer constant, k, has a value between 0.85 and 0.94, and β is the half diffraction angle minus the Bragg angle. The ternary composite's mean crystal size was 36 nm. This indicates that the material exhibits significant crystallinity at the nanoscale. The small crystal size can influence the material's properties, such as its mechanical strength and thermal stability, making it suitable for various advanced applications in nanotechnology and materials science.

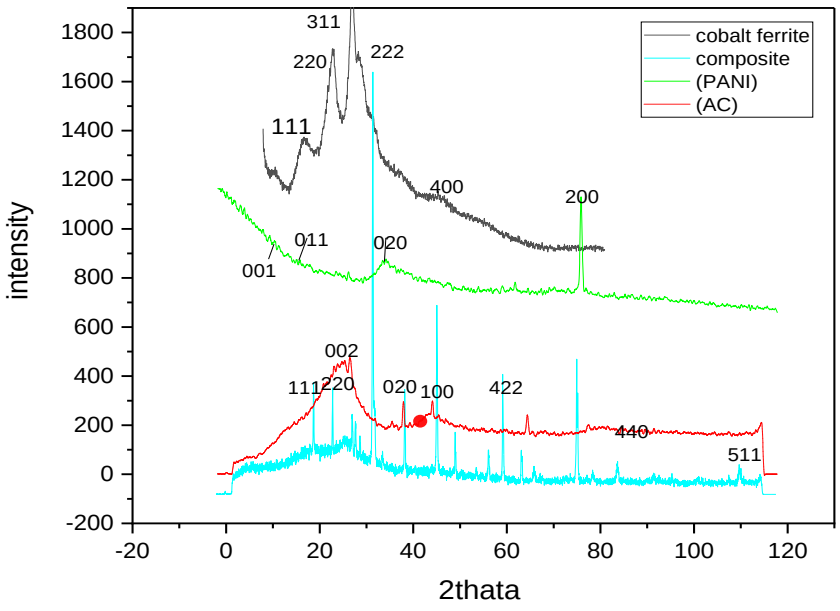

Figure 3. XRD spectra of $CoFe_2O_4$/AC/PANI NPs and composite.

Pore size distribution BET analysis

Using the nitrogen adsorption-desorption isotherm, the BET surface areas and pore size distribution of $CoFe_2O_4$/AC/PANI NPs nanocomposite were determined, according to the BET theory, as displayed in Figure (4) that demonstrates the hysteresis loops with adsorption isotherms is type IV. The hysteresis loop was shown to be of type H3 in the relative pressure (P/P_0) range of 0.3–1.0 [22,23] The $CoFe_2O_4$/AC/ PANI nanocomposite's anticipated pores are spherically closed [24]. Based on the data, the $CoFe_2O_4$/AC/ PANI nanocomposite has a specific surface area of 54.118 m^2/g^{-1} and total pore volume are equal to 0.05046 $cm3.g^{-1}$, while according to the BJH isotherm, the mean pore diameters of $CoFe_2O_4$/AC/ PANI is 9.4355 nm, this result is assessed as a meso-porous between (2-50 nm) [25,26]

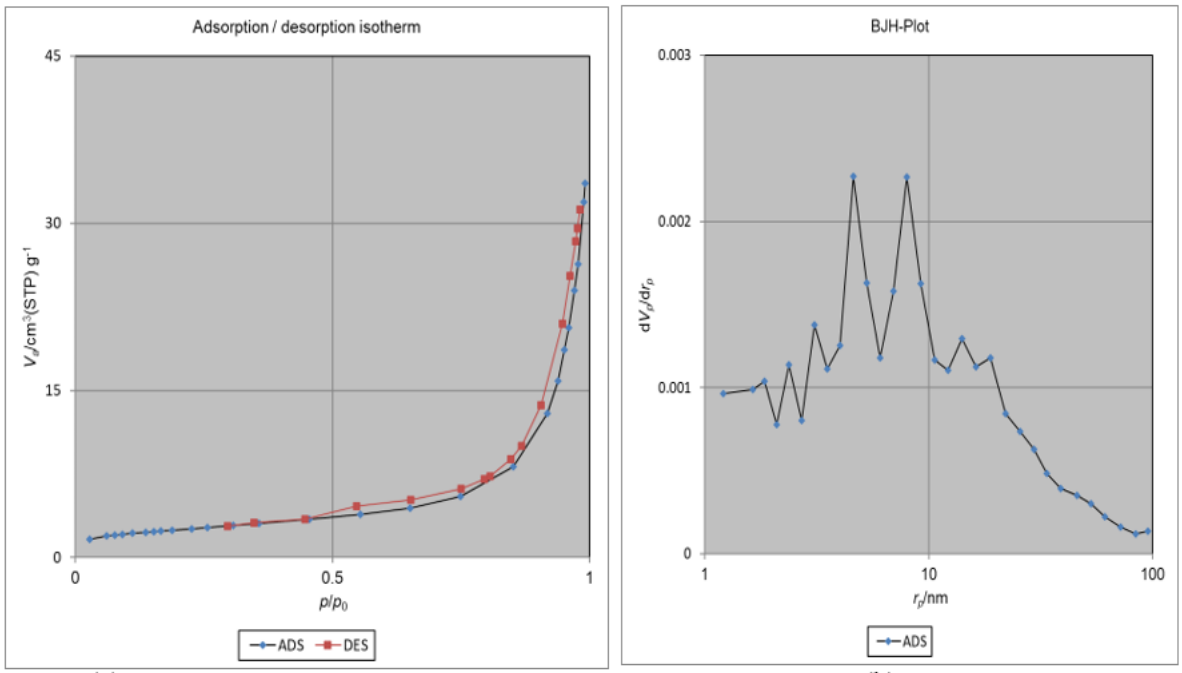

Figure 4. N_2 Adsorption - desorption analysis of $CoFe_2O_4$/AC/ PANI composite (a) BET plots (b) BJH pore size distribution

Analysis of zeta potential

A liquid environment measurement of surface electrical charge defines zeta potential for dispersed particles. The stability of the colloidal system directly correlates with the measured zeta potential that produces strong inter-particle repulsion when the values are above ±30 mV, but exhibits aggregation-flocculation tendencies when the values fall below ±10 mV. Measurement conditions[27]. Depended on figure 5 and table 1, the results indicate that the particles in the ternary composite ($CoFe_2O_4$/AC/ PANI composite) have a positive surface charge (20.2 mV), giving them relative stability in aqueous media.

Table 1. Results of Zeta Potential of $CoFe_2O_4$/AC/ PANI composite

Info.	Values
Zeta Potential	**20.2 mV**
Electrophoretic Mobility	0.000157 cm^2/Vs
Temperature	25.2 °C
Viscosity	0.892 mPa·s
Conductivity	0.220 ms /cm

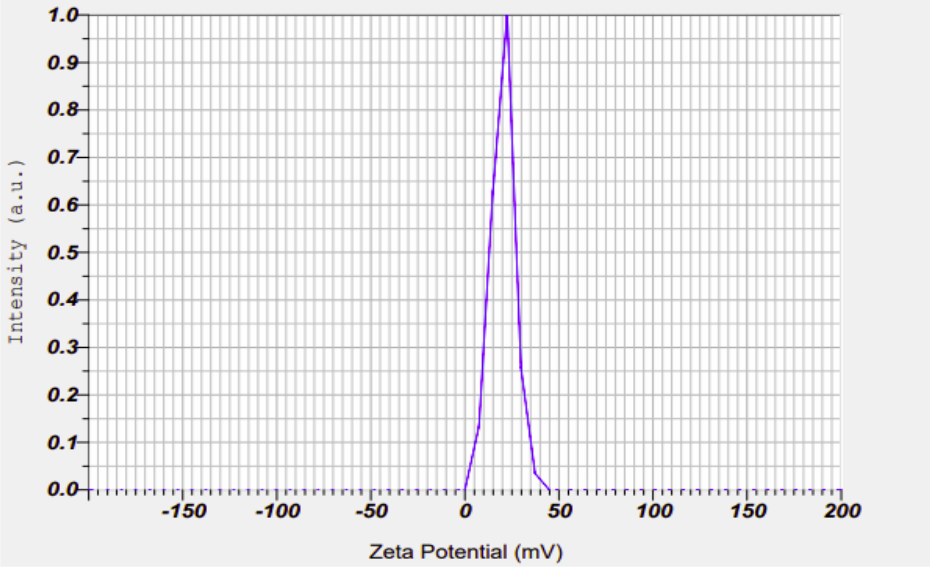

Figure 5. Zeta Potential (mV) of $CoFe_2O_4$/AC/PANI NPs composite.

Scanning Electron Microscopy (SEM) Analysis

The particle sizes in figure 6 ranges from 33.74 nm to 49.53 nm with agglomerated as layers. The micrographs of the composite films clearly indicated that the activated carbon and cobalt ferrite particles were well dispersed in the composite films. This uniform distribution of particles contributes to the enhanced mechanical properties and thermal stability of the films, making them suitable for various applications in nanotechnology and material science. Additionally, the presence of these particles was found to improve the electrical conductivity of the composite films significantly[28,29].

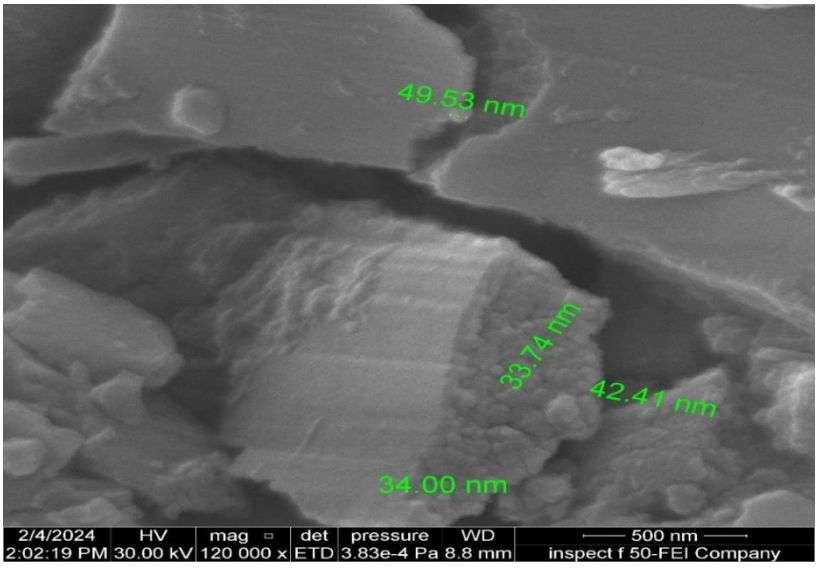

Figure 6.The scanning electron microscope of $CoFe_2O_4$/AC/PANI NPs composite.

EDX analysis of $CoFe_2O_4$/AC/ PANI composite

The elemental composition was analyzed by energy dispersive X-ray (EDX) analysis and found the C and N elements come from polyaniline and active carbon, while the Co, Fe and O conform the linked $CoFe_2O_4$ with AC and PANI, as seen in Figure 7 .

\

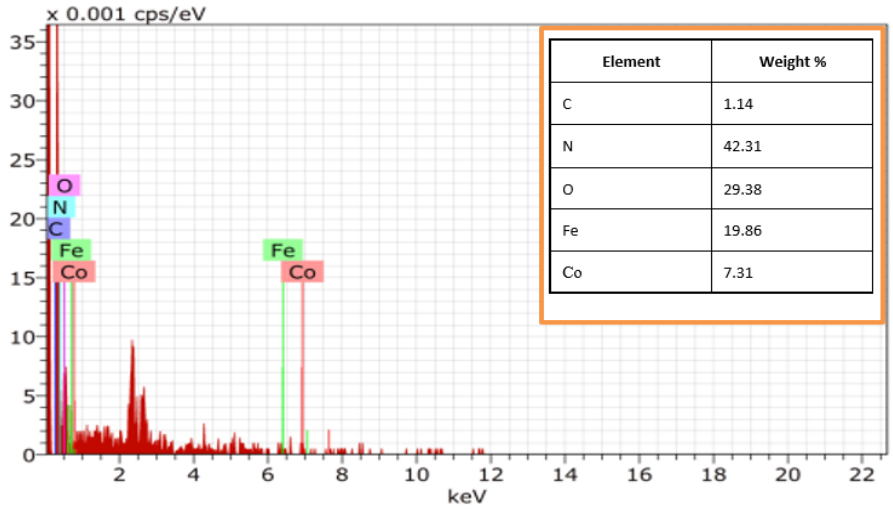

Figure 7. EDX spectrum of $CoFe_2O_4$/AC/PAIN composite.

Adsorption activity evaluation

The Adsorption activity study was performed using by filling various volumetric flasks with 25 mL of each of the adsorption solutions of direct orange 39 dye at concentrations ranging from 5, 10, and 15 ppm. These flasks were placed in a water bath with a vibrator at a varied temperature between 283-298 K after these solutions were in contact with (0.1,0.2,0.3,0.4) g of adsorbent surface ($CoFe_2O_4$/AC/PANI NPs). The pH (4,5,6,7,9, and 11) was used to regulate the acid function for improving the uptake of dye. The amount of adsorption was then determined when the flasks were removed at contact durations ranging from 15 to 60 minutes. Following the adsorption process, the amount of dye residue in solution was determined at the maximum wavelength (λmax), which is 416 nm. Thermodynamic investigations were conducted in stages to determine optimal conditions and temperatures. The adsorption (Removal) efficiency E % can be calculated by following the equation [30-32].

$$\boldsymbol{Removal\ offeciency}\ (\boldsymbol{E}\ \%) = \frac{\boldsymbol{C_o - C_e}}{\boldsymbol{C_o}} \times \mathbf{100} \qquad \mathbf{(2)}$$

Where: C_O, Ce Indicate to the starting concentration and equilibrium concentration of residual dye mg/L.

Effect of Contact Time

Total equilibrium time requires to detect the uptake reaction kinetic that evaluated the adsorption order. For an effective adsorption method, both the initial equilibrium reaction time must be quick and equilibrium must establish itself with maximum adsorption bias. The removal rate of direct orange 39 dye was uptake from the solution using $CoFe_2O_4$/AC/ PANI nanocomposite depends on reaction time, as demonstrated in Fig. 8. The reaction started with fast adsorption during the initial 15- 45 minutes because of diffusion the dye molecule on surface then likes on active sites. The removal efficiency showed minimal change after 45 min because the active sites already occupied that reached it to the equilibrium [10]. The brief reaction duration reached completion at 45 minutes with E% 95.246 according to the illustration data; therefore, 45 minutes represents the most suitable adsorption period for the dye on $CoFe_2O_4$/AC/ PANI nano-composite surface.

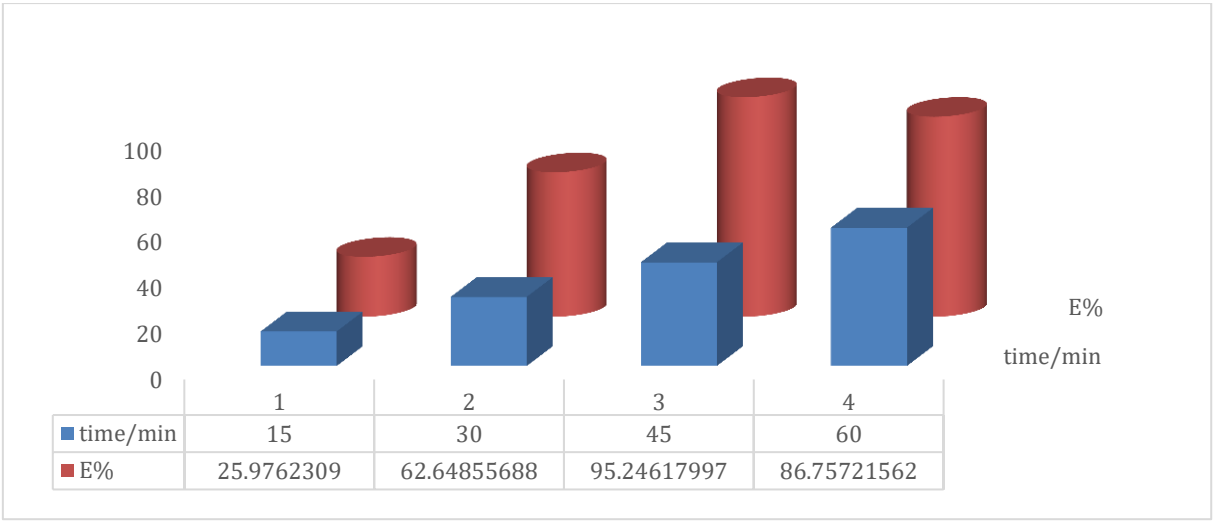

	1	2	3	4
time/min	15	30	45	60
E%	25.9762309	62.64855688	95.24617997	86.75721562

Figure 8. Relationship between E% and time (min) for adsorption of direct orange 39 dye on synthesized composite nanoparticles, (conditions: pH 6; dosage= 0.025 g; 5 ppm of dye, V=50 mL; time=(15-60) min; T=298 K)

Kinetic of dye adsorption on $CoFe_2O_4$/AC/ PANI nanocomposite

The linear form of the pseudo-first order (PFO) was employed in equation 6, to find adsorption rate constants (k1) in min^{-1} [33].

$$\ln(qe - qt) = \ln qe - k1t \qquad (6)$$

When qe is the adsorption capacity of dye on $CoFe_2O_4$/AC/ PANI nanocomposite at equilibrium ($mg.g^{-1}$), qt is the adsorption capacity at time t ($mg.g^{-1}$),t is time of contact. The PFO model's are

defined by k1 (min), whose magnitude can be determined from the linear plots of ln(qe-qt) against t (Fig. 9 a) and the results shown in Table 3. Clearly, lower correlation coefficients (R^2) were found, indicating that the PFO model does fully obey the experimental results of the adsorption method as mentioned in previous studies[34-36]. After that, a pseudo-second-order (PSO) kinetics model was used to confirm the findings.

$$\frac{1}{qe} = \frac{1}{k2q2e} + \frac{t}{qt} \qquad (7)$$

For PSO kinetic models at 298 K, the rate constants are expressed by k2 (mg/g. min) from Equation (7). As illustrated in Fig. 13b, the intercept and gradient of the plot of t/qt against t can be used to calculate both k2 and qe.

Based on table 3, The PFO model is obeyed the adsorption of direct orange 39 dye onto the $CoFe_2O_4$ /AC/ PANI nanocomposite adsorbent, because correlation coefficient R^2 for PFO > correlation coefficient R^2 for PSO this really case in adsorption process and agreement with the result reported in study for Kinetic study of the adsorption of dyes onto activated carbon by Eris and Bashiri[34]. Moreover, Simonescu and coworker [37], found the PFO model is more feasible applicable for the removal of anionic dyes Methyl Orange (MO),using $CoFe_2O_4$.

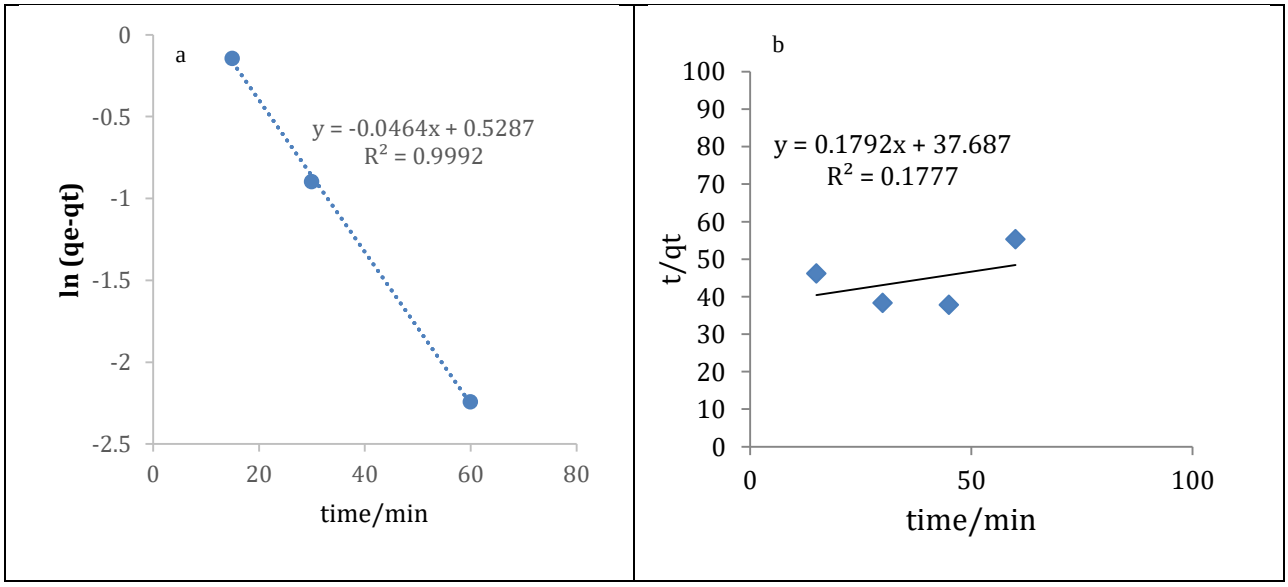

Figure 9. a) pseudo-first order kinetic model, b) second order for adsorption of direct orange 39 dye on the composite surface, (conditions: pH 6; dosage of composite = 0.025 g; V=50 mL; time=45 min, concentration of dye 5 mg/L, at T=298 K).

Table 3. The kinetic constants and correlation coefficients for both models.

Samples	Pseudo-first order			Pseudo-second order		
	$k_{1\ (min^{-1})}$	q_e (mg g^{-1})	R^2	k_2 ($L\ min^{-1}\ mol^{-1}$)	q_e (mg g^{-1})	R^2
Composite	0.036	1.696725132	0.9992	0.0788097	5.580357	0.1777

Impact of direct orange 39 concentration on removal process using $CoFe_2O_4$/AC/ PANI nanocomposite

According to Fig. 10, the effect of direct orange 39 dye concentration on removal tests using $CoFe_2O_4$/AC/ PANI nanocomposite explains at different initial concentrations from 5 to 15 mg/L. The result in this figure indicates that reducing dye initial concentrations led to higher percentages of removal. In other word, at minimal initial concentrations, the cordial interactions between direct orange 39 dye molecules and the surface of $CoFe_2O_4$/AC/ PANI nanocomposite denoted their initial high strength, but they declined when the initial concentration rose since active monolayer adsorption sites on each adsorbent ran out [28-31].

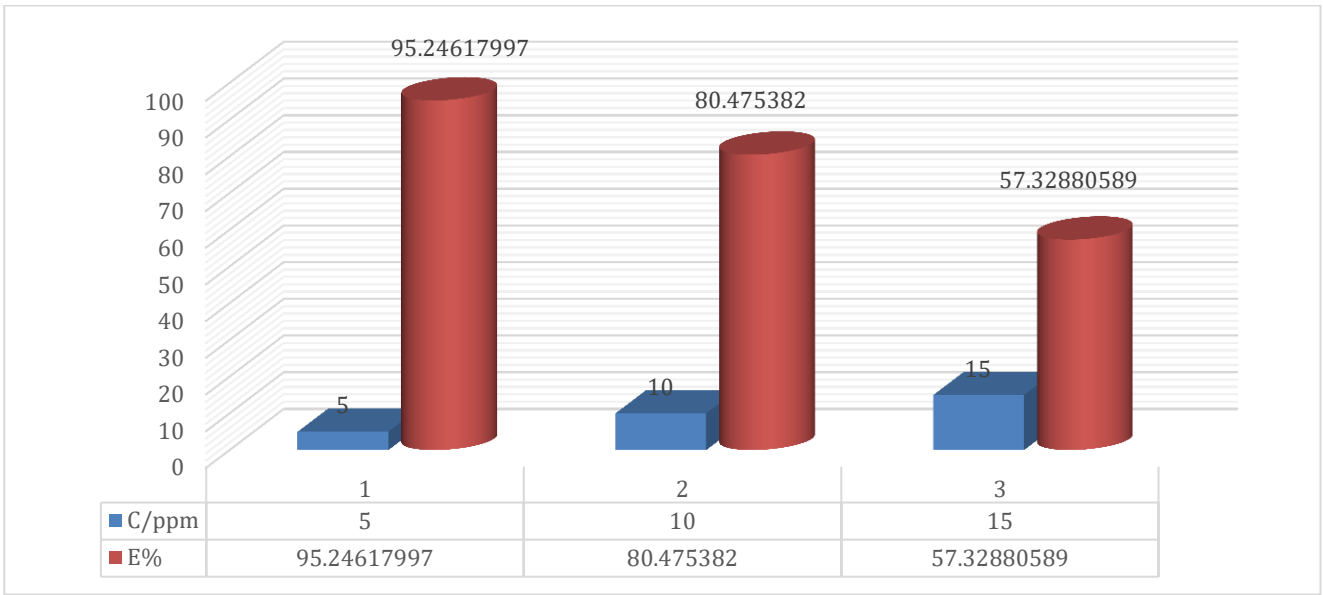

Figure 10. Relationship between(E%) and different concentrations of dye (C/ppm), (conditions: pH 6; dosage of composite = 0.0255 g; V=50 mL; time=45 min, concentration of dye= (5-15) mg/L, at T=298 K).

Effect of pH of direct orange dye

The altering pH in dye solution deems a crucial factor via dye removal process in different solution media. The figure 11 shows effect of pH of direct orange dye. The removal efficiency elevates with raising the pH of dye solution reached to pH 6 with the maximum dye removal of 95.246%, then decreases because the surface of composite in basic media will be negative and the dye is acidic therefore increased in repulsion electrostatic force with surface. occurred at pH equal 6. The exposed behavior for this effect coincides with the acid-base identity of the dye solution and natural of adsorbent (composite) surface. In general, the solution pH controls on the ionization state of different dyes because this fundamental property changes both adsorption reaction speeds and adsorption equilibrium properties during the process of adsorption [29].

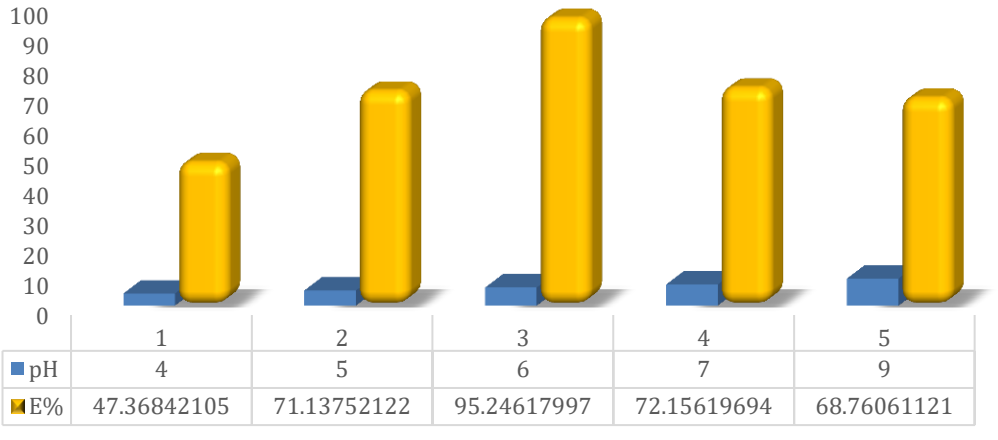

	1	2	3	4	5
pH	4	5	6	7	9
E%	47.36842105	71.13752122	95.24617997	72.15619694	68.76061121

Figure 11. Effect of change pH on removal of direct orange 39 dye using composite, (conditions: pH 9-4; dosage= 0.025 g; V= 50 mL; time = 45 min, concentration of dye 5 mg/L, at T=298 K),

Temperature's impact on the immediate removal of orange39 dye,

The temperature of reaction is wide interested with performing of the adsorption process. Figure 12 illustrates the effect of temperature on the removal of the direct orange 39 dye using the $CoFe_2O_4$/AC/PANI nanocomposites. It may be concluded that when the temperature rises from 298 to 310 K, the removal efficiency (E%) ranged from 59.252 to 95.246%. Therefore, this study's methodology is endothermal in origin [30-32].

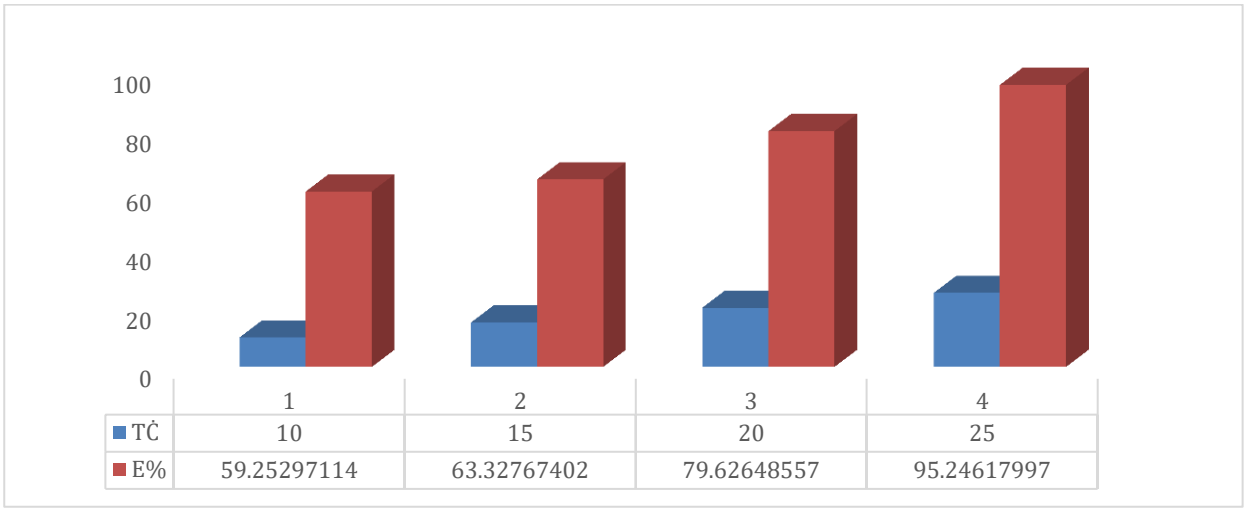

Figure 12. Effect of temperature on removal efficiency of the direct orange 39 dye using composite, (conditions: pH 6; dosage = 0.025 g; V=50 mL; time=45 min, concentration of dye 5 mg/L and temperature = (10-25) ^{o}C.

Thermodynamic parameter.

The thermodynamic analysis is required to explain the adsorption's nature process. Standard enthalpy change (ΔH^{o} (J/mol)), standard entropy change (ΔS^{o} (J/mol K)), and changes in standard Gibbs free energy (ΔG^{o} (kJ/mol)) are some of the variables that describe a method's thermodynamic behavior. The Vant Hoff equation [29]was used to estimate ΔH^{o} and ΔS^{o}, as seen figure 13a and table 2.

$$\ln k_d = \frac{-\Delta H^{\circ}}{RT} + \frac{\Delta s^{\circ}}{R} \qquad (3)$$

Here, k_d is adsorption constant, R is universal gas constant (8.314 J/mol K) and T is absolute temperature (K).

ΔG^{o} was calculated using Nernst Equation [38,39], as displayed in figure 13 b and table 2.

$$\Delta G^{o} = -RT ln k_d \qquad (4)$$

Activation energy (E_a) provides information regarding the kind of adsorption, including the reaction is fast or slow. The E_a for this adsorption system was calculated:[34-35]

$$E_a = \Delta H^{o} + RT \qquad (5)$$

Here, Ea is activation energy (the amount of energy needed to start a reaction), $\Delta H\circ$is enthalpy change of reaction, R is universal gas constant (8.314 J/mol·K) and T is the Kelvin temperature.

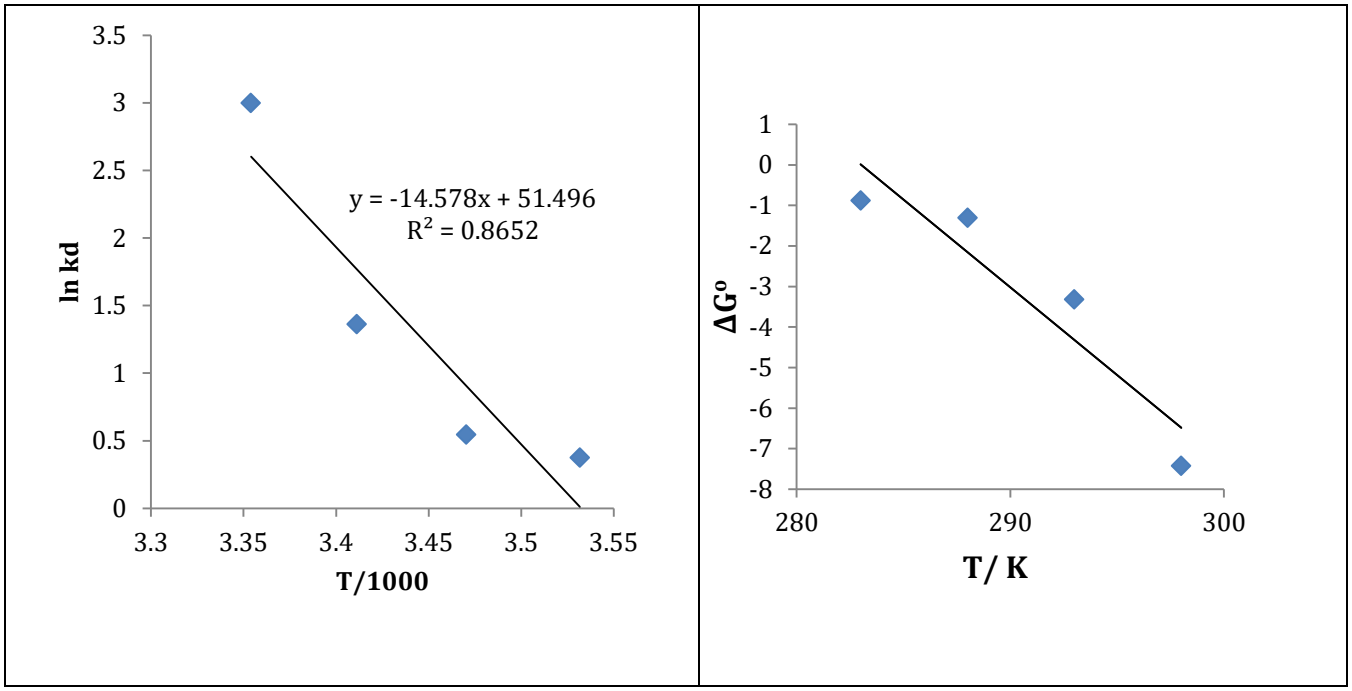

Figure 13.a) Relationship between lnk_d and 1000/T during direct orange 39 dye removing via $CoFe_2O_4$/AC/ PANI NPs,b) The variability of Gibb's free energy changes (ΔG) for direct orange 39 dye removing from the $CoFe_2O_4$/AC/ PANI surface at various temperatures. (conditions: pH 6; dosage = 0.025 g; V=50 mL; time=45 min, concentration of dye 5 mg/L, at T=283-298 K).

Table 2. Kinetic and thermodynamic variables for adsorption of direct orange 39 dyes on composite surfaces.

T/K	ΔH^o kJ mol^{-1}	ΔS^o kJ mol^{-1}	ΔG^o kJ mol^{-1}	E_a kJ mol^{-1}
283	121.2015	**0.428138**	**-0.88099**	**123.55**
288			-1.30808	**123.60**
293			-3.32054	**123.64**
298			**-7.42656**	**123.68**

Based on Figure13 and Table 2 elucidates the thermodynamic parameters predominated on the adsorption manner. The Gibbs free energy (ΔG^o) values are negative indicating the adsorption of direct orange 39 dye by composite is a spontaneous reaction. The positive ΔH^o of this reaction was found to be 121.2015 kJ/mol, this value suggests that the adsorption type is chemical (higher 80

kJ/mol) and the system is endothermic [40-43]. Furthermore, the small value of ΔS^{o} (0.428138 kJ/mol. K) ensures the decline in the randomness of the solid-solution interface in the course of the adsorption system [44]. The values of activation energy ensure the uptake of dye from solution to composite surface successfully happened.

Reusability of composite nanoparticles

The statistics provided in Figure (14) shed mild on the reusability of the synthesized composite NPs for packages. While the nanoparticles exhibited an impressive 97.48 % removal efficiency performance in the preliminary cycle, a gradual decline in performance was found with subsequent reuse cycles. This phenomenon can be ascribed to the capacity deactivation by saturated or blocking the active sites of surface by dye molecules, or fouling of the nanoparticle surface, which may restrict the adsorption and adsorption strategies[45]. Nevertheless, the nanoparticle's proven ability to perform well during the first three rounds pastime more than one cycle underscores their potential for sustainable and fee-effective applications. The results indicate a decline in adsorption efficiency with a continuous reuse cycle when used five times. it maintained its warranty until the third time because the dye molecules are gradually accumulating and preventing interaction with the surface[46]. However, the nanoparticles still exhibited significant adsorption activity after multiple cycles. The results observed good reusability, which is the acceptable loss in the sorption ability after five circulations.

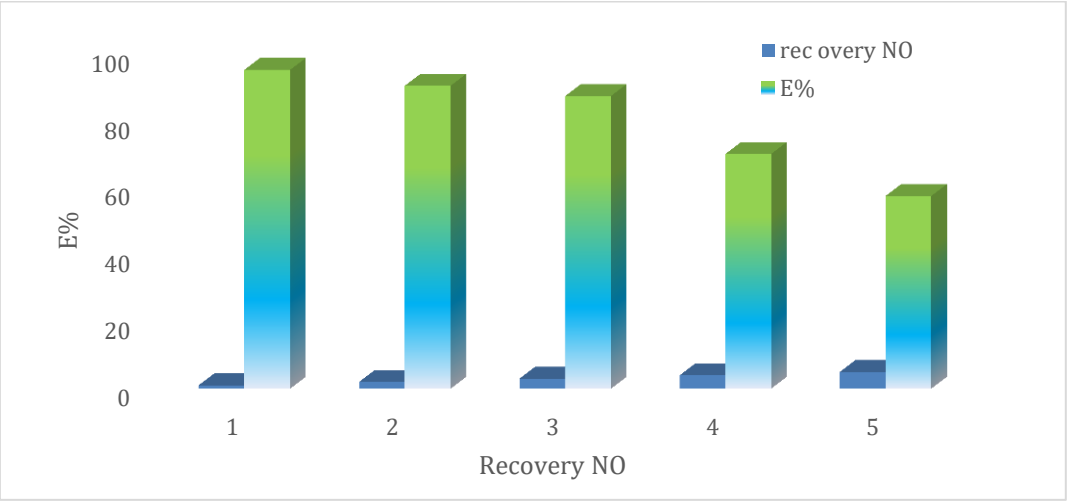

Figur 15. Adsorption cycles of direct orange dye adsorption by the $CoFe_2O_4$/AC/ PANI nanocomposite adsorbent, (conditions: pH 6; dosage = 0.025 g; V=50 mL; time=45 min, concentration of dye = 5 mg/L, at T=298 K).

Conclusion

$CoFe_2O_4$/AC/ PANI Nanoparticle Synthesis. FT-IR, XRD, BET and zeta potential technique were used to analyze and confirm the synthesized ternary composite nanoparticles, FTIR spectroscopy of the $CoFe_2O_4$/AC/ PANI complex shows the appearance of new peaks at 1513.08 and 470.65 cm^{-1}, indicating chemical interactions between the three components. This shows the formation of new bonds, which affects the vibrational structure of Fe–O and Co–O. These changes enhance the functional properties of the compound in removal direct orange 39 dye. The produced particles had an average diameter of 36 nm respectively. They were also stable. The $CoFe_2O_4$/AC/ PANI composite has a high surface area of 54.118 m^2/g^{-1} and mesopore porosity with an average diameter of 9.4355 nm, facilitating the access of reactants to the active sites. These properties enhance its efficiency in catalytic and adsorption applications compared to other materials. The composite was used to extract the basic direct orange 39 dye from an aqueous solution due to their adsorption activity. direct orange 39 dye was effectively removed from water by employing produced ternary composite NPs as an adsorbent substance. 6. At 45 minutes and pH 6, 0.025g of adsorbent surface weight combined with 5ppm of direct orange 39 dye solutions had the greatest adsorption efficiency, The results indicate that the particles in the ternary complex have a positive surface charge (20.2 mV), giving them relative stability in aqueous media. Thermodynamic studies revealed that sorption of dye on to composite was done, and the enthalpies (ΔH) were 121.2015kJ/mol This means that the adsorption is in $CoFe_2O_4$/AC/ PANI, be chemical.

Acknowledgments: The authors would like to thank all supported people at the University of Karbala and Al-Zahraa Center for Medical and Pharmaceutical Research Sciences (ZCMRS), Al-Zahraa University for Women.

Conflict of Interest: The authors declare no conflict of interest.

References

[1] Mgbemene, C.A. (2011). The effects of industrialization on climate change, in *Fulbright Alumni Association of Nigeria 10th Anniversary Conference Development, Environment and Climate Change: Challenges for Nigeria, University of Ibadan*, pp. 12–15 DOI: 10.3923/jest.2016.301.316.

[2] Ebenstein, A. (2012). The consequences of industrialization: evidence from water pollution and digestive cancers in China," *Rev. Econ. Stat.*, 94(1), pp. 186–201 DOI:

10.1162/REST_a_00150.

[3] Schwarzenbach, R.P., Egli, T., Hofstetter, T.B., Von Gunten, U. and Wehrli, B. (2010) Global water pollution and human health, *Annu. Rev. Environ. Resour.*, 35, pp. 109–136. doi.10.1146/annurev-environ-100809-125342.

[4] Azizullah, A., Khattak, M.N.K., Richter, P. and Häder, D.-P. (2011). Water pollution in Pakistan and its impact on public health—a review, *Environ. Int.*, 37(2), pp. 479–497. doi.10.1016/j.envint.2010.10.007.

[5] Kant, R. (2012). Textile dyeing industry: an environmental hazard, *Natural Science,*.4(1)*, pp. 22-26* . DOI: 10.4236/ns.2012.41004.

[6] Turki, Z.T. (2024). The effect of avocado peel extract on the optical properties of cadmium sulfide nanostructures," *Al-Zahraa J. Heal. Med. Sci.*, 2(2), pp. 80–84.

[7] Zhang, W., Liu, J.X., Zhang, Y., Yu, Y., Zheng, Y., Liu, Z., Li, Y. and Qi, Q. (2022) "The impact of cyanobacteria blooms on the aquatic environment and human health," *Toxins (Basel).*, 14(10), p. 658. doi.10.3390/toxins14100658.

[8] Holkar, C.R., Jadhav, A.J., Pinjari, D.V., Mahamuni, N.M. and Pandit, A.B. (2016). A critical review on textile wastewater treatments: possible approaches, *J. Environ. Manage.*, 182, pp. 351–366 /doi/10.1016/j.jenvman.2016.07.090.

[9] Lellis, B., Fávaro-Polonio, C.Z., Pamphile, J.A. and Polonio, J.C. (2019).Effects of textile dyes on health and the environment and bioremediation potential of living organisms *Biotechnol. Res. Innov.*, 3(2), pp. 275–290. doi.10.1016/j.biori.2019.09.001.

[10] Mohsin, M.E.A. and Mousa, S. (2025). Balancing Conductivity and Morphology in Aniline-Tuned Biopolymer–Starch Composites, *Polymers (Basel).*, 17(4),p. 497 doi.10.3390/polym17040497.

[11] Ali, L.A., Ismail, H.K., Alesary, H.F. and Aboul-Enein, H.Y., (2021). A nanocomposite based on polyaniline, nickel and manganese oxides for dye removal from aqueous solutions. *International Journal of Environmental Science and Technology*, *18*, pp.2031-2050. doi.10.1007/s13762-021-03194-5.

[12] Tarq, N., Sadoon, H. and Alshammari, A., (2024). Characterization of cobalt ferrite nanoparticle and evaluation its toxic effect in experimental mice: Characterization of cobalt ferrite nanoparticle and evaluation its toxic effect in experimental mice. *Acta Veterinaria Brasilica, 18*(2),pp. 103-110. **DOI:** doi.10.21708/avb.2024.18.2.12019.

[13] Ibeniaich, M., Elansary, M., Minaoui, M., Mouhib, K., El Haj, Y., Ait Belaiche, Y., Oulhakem, Y., Iffer, O., Ferdi, E., Ahmani Lemine, C. and M, O. (2024) "Exploring the effect of Hf (IV) doping in spinel ferrite $CoHfxFe_2$-xO_4 on magnetic properties, electrochemical impedance, and photocatalytic activity: In-depth structural study," *J. Mol. Struct.*, 1318, p. 139395. doi.10.1016/j.molstruc.2023.139395.

[14] Tian, Y., Fan, X., Chen, X., Chen, K., Peng, X., Wang, W., Wang, L. and Wang, F. (2024) Optical biomarker analysis for renal cell carcinoma obtained from preoperative and postoperative patients using ATR-FTIR spectroscopy, *Spectrochim. Acta Part A Mol. Biomol. Spectrosc.*, 318, p. 124426. doi.10.1016/j.saa.2024.124426.

[15] Durig, D.T. (1987). Conformational analysis of some halo or pseudohalo substituted small organic molecules by spectroscopic and theoretical methods. University of South Carolina, 1987.

[16] Liu, M., Yang, X., Shao, W., Wu, T., Ji, R., Fan, B. and Tong, G. (2021) Superior microwave absorbing properties of O, S, N codoped carbon planar helixes via carbonization of polypyrrole spiral nanowires, *Carbon N. Y.*, 174, pp. 625–637doi.10.1016/j.carbon.2020.11.093.

[17] Kalam, A., Al-Sehemi, A.G., Assiri, M., Du, G., Ahmad, T., Ahmad, I. and Pannipara, M., (2018). Modified solvothermal synthesis of cobalt ferrite ($CoFe_2O_4$) magnetic nanoparticles photocatalysts for degradation of methylene blue with H_2O_2/visible light. *Results in physics*, *8*, pp.1046-1053 doi.10.1016/j.rinp.2018.01.045.

[18] Taresh, B.H., Fakhri, F.H. and Ahmed, L.M. (2022). Synthesis and characterization of CuO/CeO_2 nanocomposites and investigation their photocatalytic activity," *J. Nanostructures*, 12(3), pp. 563–570.doi 10.22052/JNS.2022.03.009.

[19] Kadhim, H., Ahmed, L. and AL-Hachamii, M., (2022). Facile Synthesis of Spinel $CoCr_2O_4$ and Its Nanocomposite with ZrO_2: Employing in Photo-catalytic Decolorization of Fe (II)-(luminol-Tyrosine) Complex. *Egyptian Journal of Chemistry*, *65*(1), pp.481-488.doi 10.21608/ejchem.2021.81251.4025.

[20] Obaid, A. and Ahmed, L., (2021). One-step hydrothermal synthesis of α-MoO_3 nano-belts with ultrasonic assist for incorporating TiO_2 as a nanocomposite. *Egyptian Journal of Chemistry*, *64*(10), pp.5725-5734.doi 10.21608/ejchem.2021.72582.3615.

[21] Jaafar, M. T., Ahmed, L. M. & Haiwal, R. T. (2023). Solvent-Free Hydrothermal Synthesis

of Network-Like Graphene Quantum Dots (GQD) Nano Particle and Ultrasonic TiO_2/GQD Nanocomposite," *J. Nanostructures*, vol. 13, no. 3, pp. 626–638.doi 10.22052/JNS.2023.03.003

[22] Chang, S.-S. C., Ruelle, B., Beauchêne, J., Di Renzo, J., Quignard, F., Zhao, F., Guang-Jie, G., Yamamoto, H. & Gril, J. (2009). Mesoporosity as a new parameter for understanding tension stress generation in trees," *J. Exp. Bot.*, 60(11), pp. 3023–3030 doi.10.1093/jxb/erp133.

[23] Lowell, S., Shields, J. E., Thomas, M. A., & Thommes, M. (2012). Characterization of porous solids and powders: surface area, pore size and density (Vol. 16). Springer Science & Business Media DOI: 10.1007/978-1-4020-2303-3_18.

[24] Ambroz, F., Macdonald, T. J., Martis, V. & Parkin, I. P. (2018). "Evaluation of the BET Theory for the Characterization of Meso and Microporous MOFs," *Small methods*, 2(11), p. 1800173 doi10.1002/smtd.201800173.

[25] Prasanna, G. D., Jayanna, H. S., Lamani, A. R. & Dash, S. (2011). Polyaniline/$CoFe_2O_4$ nanocomposites: A novel synthesis, characterization and magnetic properties," *Synth. Met.*, 161(21–22), pp. 2306–2311doi.10.1016/j.synthmet.2011.07.003. DOI: 10.1016/j.synthmet.2011.07.003.

[26] Villarroel-Rocha, J., Barrera, D., Arroyo-Gómez, J. J., & Sapag, K. (2020). Critical overview of textural characterization of zeolites by gas adsorption. New Developments in Adsorption/Separation of Small Molecules by Zeolites, 31-55, doi:10.1007/430_2020_69doi.10.1007/s10450-020-00206-7.

[27] Yu, W., Batchelor-McAuley, C., Chang, X., Young, N. P. & Compton, R. G. (2019). Porosity controls the catalytic activity of platinum nanoparticles, *Phys. Chem. Chem. Phys.*, 21(36), pp. 20415–20421**DOI**doi.10.1039/C9CP03887F.

[28] Ghaffari Touran, N. (2020). Surface-chemical interactions between apatite and hematite in aqueous suspensions. University of British Columbiahttps://dx.doi.org/10.14288/1.0388358.

[29] Zengin, H. & Kalaycı, G. (2010). Synthesis and characterization of polyaniline/activated carbon composites and preparation of conductive films, *Mater. Chem. Phys.*, 120(1), pp. 46–53doi.10.1016/j.matchemphys.2009.10.019.

[30] Löwenberg, J., Zenker, A., Baggenstos, M., Koch, G., Kazner, C. and Wintgens, T., 2014. Comparison of two PAC/UF processes for the removal of micropollutants from wastewater

treatment plant effluent: Process performance and removal efficiency. Water Research, 56, pp.26-36.

[31] Vona, A., Di Martino, F., Garcia-Ivars, J., Picó, Y., Mendoza-Roca, J.A. and Iborra-Clar, M.I., 2015. Comparison of different removal techniques for selected pharmaceuticals. Journal of Water Process Engineering, 5, pp.48-57.

[32] Saeed, S. I., Taresh, B. H., Ahmed, L. M., Haboob, Z. F., Hassan, S. A. & Jassim, A. A. A. (2021). Insight into the Oxidant Agents Effect of Removal and Photodecolorization of Vitamin B 12 Solution in Drug Tablets using ZrO_2., *J. Chem. Heal. Risks*, 11(4) DOI: 10.22034/jchr.2021.685757.

[33]Simonescu, C.M., Tătăruş, A., Culiţă, D.C., Stănică, N., Ionescu, I.A., Butoi, B. and Banici, A.M., (2021). Comparative study of $CoFe_2O_4$ nanoparticles and $CoFe_2O_4$-chitosan composite for Congo red and methyl orange removal by adsorption. *Nanomaterials*, *11*(3), p.711 doi.10.3390/nano11030711.

[34] Eris, S. & Bashiri, H. (2016). Kinetic study of the adsorption of dyes onto activated carbon, *Prog. React. Kinet. Mech.*, 41(2), pp. 109–119 doi.10.3184/146867816X14570175656394.

[35] Ali, S., Ali, M. and Ahmed, L., (2021). Hybrid Phosphotungstic acid-Dopamine (PTA-DA) Like-flower Nanostructure Synthesis as a Furosemide Drug Delivery System and Kinetic Study of Drug Releasing. *EgyptianJournalof Chemistry*, *64*(10), pp.5547-5553DOI: 10.21608/ejchem.2021.75210.3692

[36] Taty-Costodes, V. C., Fauduet, H., Porte, C. & Delacroix, A. (2003). "Removal of Cd (II) and Pb (II) ions, from aqueous solutions, by adsorption onto sawdust of Pinus sylvestris," *J. Hazard. Mater.*, 105(1–3), pp. 121–142. DOI: 10.1016/j.jhazmat.2003.07.009.

[37] Simonescu, C.M., Tătăruş, A., Culiţă, D.C., Stănică, N., Butoi, B. and Kuncser, A., (2021). Facile synthesis of cobalt ferrite ($CoFe_2O_4$) nanoparticles in the presence of sodium bis (2-ethyl-hexyl) sulfosuccinate and their application in dyes removal from single and binary aqueous solutions. *Nanomaterials*, *11*(11), p.3128**DOI:** 10.3390/nano11113128.

[38] Nandiyanto, A. B. D., Putri, M. E., Fiandini, M., Ragadhita, M., Kurniawan, R., Farobie, T., Bilad, O. & R., M. (2024). Characteristics of Ammonia Adsorption on Various Sizes of Calcium Carbonate Microparticles from Chicken Eggshell Waste, Mor, *J. Chem*, 12(3), pp. 1073–1095.

[39] Jaafar, M. T. & Ahmed, L. M. (2020). Reduced the toxicity of acid black (nigrosine) dye by

removal and photocatalytic activity of TiO_2 and studying the effect of pH, temperatue, and the oxidant agents, in *AIP Conference Proceedings*, AIP Publishing. DOI: 10.1063/5.0027512

[40] Al-Fiydh, M. N., Najm, H. F., Karam, F. F. & Baqir, S. J. (2024). Thermodynamics, kinetic study and equilibrium isotherm analysis of cationic dye adsorption by ternary composite," *Results Chem.*, 10, p. 101680**DOI:** 10.1016/j.rechem.2023.101680.

[41] Mokhbi, Y., Ghiaba, Z., Akchiche, Z., Ghedamsi, R. & Recioui, B. (2024) "Study of the adsorption mechanism of certain dyes from wastewater on commercial activated carbon using the Langmuir and Freundlich methods, *Stud. Eng. Exact Sci.*, 5(2), pp. e5789–e5789DOI: 10.22052/SEES.2024.02.019

[42] Khit, S. A., Shaheed, I. M. & Kareem, E. T. (2023). A green synthesis of copper oxide nanoparticles using Anchusa strigosa L. flowers extract and study their impact for water pollutant removal, in *AIP Conference Proceedings*, AIP Publishing DOI: 10.1063/5.0097156

[43] Arampatzidou, A. C. & Deliyanni, E. A. (2016). Comparison of activation media and pyrolysis temperature for activated carbons development by pyrolysis of potato peels for effective adsorption of endocrine disruptor bisphenol-A, *J. Colloid Interface Sci.*, 466, pp. 101–112. DOI: 10.1016/j.jcis.2015.12.043.

[44] Santos, R. S., Dantas, É. F. M., Oliveira, E. J. M., Simões, E. D. C., Araújo, T. B., Ribeiro, Í. R. S., Oliveira, A. T. S., Garcia, L. P. S., Almeida, R. R. P. & Luciano, C. (2020). Potential reuse of PET waste bottles as a green substrate/adsorbent for Reactive Black 5 dye removal, *Water, Air, Soil Pollut.*, 231(1–16). DOI: 10.1007/s11270-020-04507-x.

[45] Borgohain, X., Das, E., & Rashid, M. H. (2023). Facile synthesis of Ce nanoparticles for enhanced removal of malachite green dye from an aqueous environment, *Mater. Adv.*, 4(2), pp. 683–693. **DOI**: 10.1039/D2MA01019D.

[46] Dadashi, R., Bahram, M., Farhadi, K., Asadzadeh, Z., & Hafezirad, J. (2024) Photodecoration of tungsten oxide nanoparticles onto eggshell as an ultra-fast adsorbent for removal of MB dye pollutant, *Sci. Rep.*, 14(1), p. 14478. **DOI**: 10.1039/D2MA01019D